THE JOURNAL OF PHYSICAL CHEMISTRY B

Article

pubs.acs.org/JPCB

Mechanism of the Glycosylation Step Catalyzed by Human α-Galactosidase: A QM/MM Metadynamics Study

Xiao-Liang Pan, Wei Liu, and Jing-Yao Liu*

State Key Laboratory of Theoretical and Computational Chemistry, Institute of Theoretical Chemistry, Jilin University, Changchun 130023, China

ABSTRACT: The enzyme α-galactosidase (α-GAL), a member of glycoside hydrolase family 27, catalyzes the removal of a nonreducing terminal α-galactose residue from polysaccharides, glycolipids, and glycopeptides. α-GAL is believed to have the double displacement retaining reaction mechanism. In this work, the glycosylation step catalyzed by human α-GAL was computationally simulated with quantum mechanics/molecular mechanics metadynamics. Our simulations show that the overall catalytic mechanism follows a $D_N{}^*A_N$-like mechanism, and the transition state has a oxocarbenium ion like character with a partially formed double bond between the ring oxygen and C5′ carbon atoms. In addition, the galactosyl ring of the substrate follows a conformational itinerary of $^4C_1 \rightarrow [E_3/{}^4H_3]^{\ddagger} \rightarrow {}^1S_3$ along the reaction coordinate.

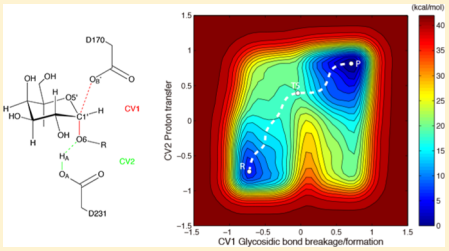

INTRODUCTION

Glycoside hydrolases (GHs) catalyze the hydrolysis of glycosidic bonds in carbohydrates. At present, GHs are classified into more than 100 families by amino acid sequence in the CAZy (Carbohydrate-Active enZYme) database.[1] α-Galactosidase (α-GAL), which belongs to GH family 27, catalyzes the removal of a nonreducing terminal α-galactose residue from polysaccharides, glycolipids, and glycopeptides. GH27 α-GALs are anomeric configuration-retaining enzymes, and thus expected to use a classical Koshland double-displacement mechanism,[2] which involves the formation of a covalent glycosyl enzyme intermediate (glycosylation step) followed by hydrolysis of this intermediate (deglycosylation step). In the glycosylation step, one carboxylic acid acts as a nucleophile and another acts as a general acid/proton donor, involving an oxacarbenium ion transition state (TS) (Figure 1).[3]

Human α-GAL is a homodimer where each monomer has two domains, an N-terminal $(\beta/\alpha)_8$ barrel containing the active site and a C-terminal antiparallel β domain.[4] Defects in human α-GAL lead to the development of Fabry disease, a lysosomal storage disorder characterized by the buildup of α-galactosylated substrates in the tissues.[5,6] Inhibitions of human α-GAL with substrate and product analogues, such as galactose[7] and 1-deoxygalactonojirimycin (DGJ),[8,9] have shown promise in pharmacological chaperone therapy for Fabry disease. Recently, Garman and co-workers determined a series of crystal structures representing each stage in the catalytic cycle of α-GAL including a covalent intermediate and suggested the conformational itinerary that the galactosyl ring of the substrate follows during catalysis.[10] On the basis of this, they proposed two new classes of inhibitors for human α-GAL, namely, TS and covalent intermediate analogues, which could be promising candidates for pharmacological chaperone therapy through tighter bindings in the active site.

In recent years, extensive theoretical studies have been devoted to the catalytic mechanism of glycoside hydrolases (retaining: family 1,[11] 2,[12−14] 5,[15,16] 7,[17−19] 11,[20−23] 12,[16] 16,[24] 18,[25] 20,[26] 22,[27,28] 38,[29] 84;[30,31] inverting: family 8,[32] 43,[33] 48,[34] 97[35]), especially the conformational itineraries which have great implications for the design of mechanism-based inhibitors for the enzyme.[36] Specifically, structural/electronic information for the glycosylation reaction TS, of interest in designing inhibitors for glycoside hydrolases, is very difficult to obtain experimentally due to the short-lived nature of the species. Computational approaches can be very useful to obtain this information. To the best of our knowledge, the catalytic mechanism of human α-GAL has not yet been addressed by theoretical studies. We report here a quantum mechanics/molecular mechanics (QM/MM) metadynamics simulation of the human α-GAL-catalyzed glycosylation reaction during the hydrolysis of a glycosidic bond. Our study presents strong hypotheses regarding the molecular/electronic details of the mechanism, specifically the conformational itinerary that the galactosyl ring follows during catalysis, the type of mechanism, and the structural/electronic properties of the TS.

COMPUTATIONAL METHODS

QM/MM Molecular Dynamics. The initial structure for the simulation was taken from a recently published X-ray crystal structure of human α-galactosidase[10] (PDB 3HG3) at 1.9 Å resolution complexed with its natural substrate and with its catalytic nucleophile mutated (D170A). The enzyme was modeled as a dimer as in the crystal structure, and all the crystallographic water molecules were kept. The D170A

Received: September 3, 2012
Revised: December 18, 2012

dx.doi.org/10.1021/jp308747c | J. Phys. Chem. B XXXX, XXX, XXX−XXX

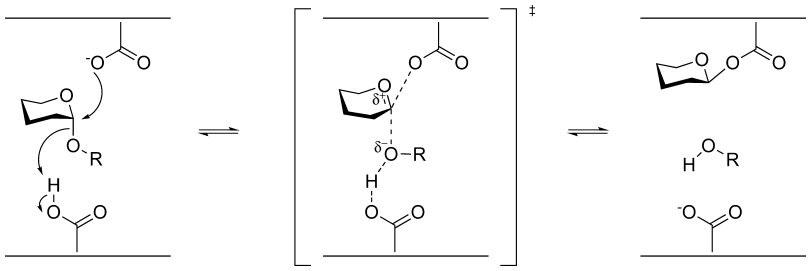

Figure 1. Schematic view of the catalytic mechanism of the glycosylation step in retaining α-GHs. The nucleophile and acid/base residues of human α-GAL are Asp170 and Asp231, respectively.

mutation of the crystal structure was manually changed back to aspartic acid. The missing hydrogen atoms were added by the Protein Preparation Wizard module of Maestro,[37] while the protonation states of ionizable amino acid residues were predicted by PROPKA.[38] The catalytic acid/base, Asp231, was modeled in its protonated state, while Asp170 was modeled in its deprotonated, charged state, consistent with the glycosylation step of the retaining mechanism. The resulting complex was solvated into a periodic rectangular water box with a buffer distance of 10 Å between each wall and the closest atom in each direction. Nine sodium ions were added to the system to neutralize the charge. These procedures led to a system of ~130 000 atoms for the QM/MM molecular dynamics (MD) simulation.

QM/MM MD simulations with periodic boundary conditions were performed using SANDER which is part of the AMBER12[39] suite of programs. The QM region was described by the PM6 method[40] augmented with an empirical dispersion correction following the formalism for DFT-D[41] (PM6-D), and consisted of the melibiose substrate, which is a reducing disaccharide formed by an alpha-1,6 linkage between galactose and glucose (D-Gal-α(1→6)-D-Glc), the side chains of the catalytic residues Asp170 and Asp231, and two hydrogen link atoms. The Amber ff12SB force field, which includes revised backbone and side chain torsion parameters over ff99SB,[42,43] was used to model the protein, and the GLYCAM06[44] force field was used to model the melibiose substrate. The water molecules were modeled with the TIP3P model.[45] A 10 Å cutoff was introduced for nonbonding interactions. The particle mesh Ewald (PME) method[46] was employed to treat long-range electrostatic interactions, and the SHAKE algorithm[47] was used to constrain all bonds involving hydrogens within the MM region. The system was minimized and then slowly heated to 300 K over 50 ps using a Langevin thermostat. Subsequently, the systems were equilibrated at 1 atm in the NPT ensemble for 450 ps. A time step of 0.5 fs was used for all the QM/MM MD simulations.

QM/MM Metadynamics. The metadynamics technique[48] was used to overcome energy barriers and to reconstruct the free energy landscape of the glycosylation reaction. A snapshot of the equilibrated system was used as the starting point for the QM/MM metadynamics simulations. The collective variables (CVs) were taken as a difference of coordination numbers (CNs) of the covalent bonds being formed/broken. The CN between two atoms i and j is defined by

$$\mathrm{CN}_{ij} = \frac{1 - (d_{ij}/d_0)^p}{1 - (d_{ij}/d_0)^{p+q}}$$

where d_{ij} is the internuclear distance of the atoms involved, d_0 is the threshold distance for bonding, and p and q are exponents that determine the steepness of the decay of CN_{ij} with respect to d_{ij}. CN values range from 0 (no bond) to 1 (a bond). Two CVs were used to indicate reaction progress (Figure 2). CV1 is

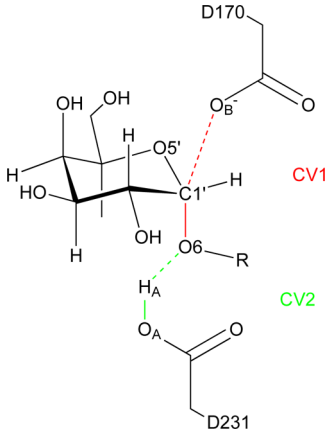

Figure 2. Collective variables (CV1 in red and CV2 in green) used to model hydrolysis of the glycosidic bond catalyzed by human α-galactosidase.

$\mathrm{CN}_{\mathrm{C1',O_B}} - \mathrm{CN}_{\mathrm{C1',O_6}}$, a measure of the formation of the E−S bond (i.e., the bond involving the anomeric carbon and the Asp170 oxygen) and the breakage of the scissile glycosidic bond (i.e., the bond between the anomeric carbon and the glycosidic oxygen). CV2 is $\mathrm{CN}_{\mathrm{H_A,O_6}} - \mathrm{CN}_{\mathrm{H_A,O_A}}$, which indicates proton transfer between the proton donor and the glycosidic oxygen atom. The selected metadynamics parameters for each of the CVs were chosen as follows: CV1, p = 12, q = 14, d_0 = 1.60; CV2, p = 12, q = 14, d_0 = 1.10. In this way, both CVs take negative values in the E·S Michaelis complex configuration and positive values in the E−S covalent intermediate configuration. Transient configurations halfway between the bonds' formation and cleavage will be reflected with CV values around 0. Gaussian hills, 1.0 kcal·mol^{-1} high and 0.15 (in units of CVs) wide, were added to the potential well every 200 MD steps. The heights of these were small enough to ensure that the calculated free-energy surface is accurate. Energy walls at CV1 = [−0.9:0.9] and CV2 = [−0.9:0.9] were added to avoid escape of the leaving group during the metadynamics simulation. The simulation was stopped after 70 ps of simulation when the system reached the product side for the second time and a total of 700 Gaussian hills had been deposited. Then, we localized the minimum free energy path (MFEP) connecting the reactant well with the product well in the two-dimensional free energy surface (FES) obtained with the metadynamics simulation

dx.doi.org/10.1021/jp308747c | J. Phys. Chem. B XXXX, XXX, XXX−XXX

using the procedures proposed by Ensing et al.[49] The metadynamics calculations were performed by interfacing the PLUMED[50] 1.3 package with AMBER.

RESULTS AND DISCUSSION

Validation of PM6-D. The validity for the PM6 method has been assessed by several previous studies. The PM6-D method, which is PM6 with dispersion correction, systematically improves all dispersion-bonded complexes over the PM6 method, yielding an accuracy close to that of high-level correlated QM methods.[51] For the particular system in this work, we have fully optimized the melibiose structure at the RI-MP2/cc-pVTZ level[52] of theory and compared it in Table 1

Table 1. Comparison of Selected Geometries between RI-MP2/cc-pVTZ, PM6, and PM6-D Optimized Melibiose Structures

	RI-MP2/cc-pVTZ	PM6	PM6-D
C1′−O6 (Å)	1.41	1.44	1.44
C6−O6 (Å)	1.42	1.45	1.45
C1′−O6−C6 (deg)	113.4	114.7	115.3

with that obtained from the PM6 and PM6-D optimization with the convergence criterion that the rms gradient is less than 0.01 kcal·mol^{-1}·Å^{-2}. The geometry differences with RI-MP2 results are about 0.03 Å for bond distances and 2.0° for bond angles for the PM6-D method. Such small differences indicate that the PM6-D method is reliable for describing geometries for relevant molecules. The RI-MP2 calculations were performed using the TURBOMOLE program.[53]

QM/MM Molecular Dynamics Simulation. QM/MM MD was performed on the model of enzyme−substrate complex built on the crystal structure. The overall structure after the simulation is very similar to the original crystal structure, with a RMSD of 1.01 ± 0.05 Å for the backbone atoms of the enzyme (averaged over the last 200 ps trajectory of the simulation). The melibiose molecule remains bound to the active site and the galactosyl ring of the substrate remains in $^4C_1$ conformation during the calculation, as in the crystal structure in spite of the fact that the mutation D170A in the crystal structure was reverted in the simulation. Throughout the simulation, there is a hydrogen bonding interaction between the proton donor Asp231 and the equatorial OH group on C2′, which may help in anchoring the relative position of the galactosyl ring of the substrate in the active site.

QM/MM Metadynamics Simulation. The first step of the enzymatic hydrolysis of the melibiose substrate by human α-GAL was modeled by QM/MM metadynamics using two CVs (see Methods section). The first variable (CV1 or nucleophilic attack) measures the degree of formation of the covalent bond between the substrate and the nucleophilic residue. The second variable (CV2 or proton transfer) quantifies the degree of proton transfer between the acid/base residue and the substrate glycosidic oxygen (Figure 2). The FES was reconstructed from the Gaussian hills added during the metadynamics simulation (Figure 3). Two local minima can be identified. The one on the left-hand side of the diagram (**R**) corresponds to the reactant state (the Michaelis complex), whereas the minimum on the right-hand side (**P**) correspond to the product state (the covalent glycosyl−enzyme intermediate). The MFEP connecting the reactant and product states was located on the FES, and the TS was identified as the maximal energy point along the

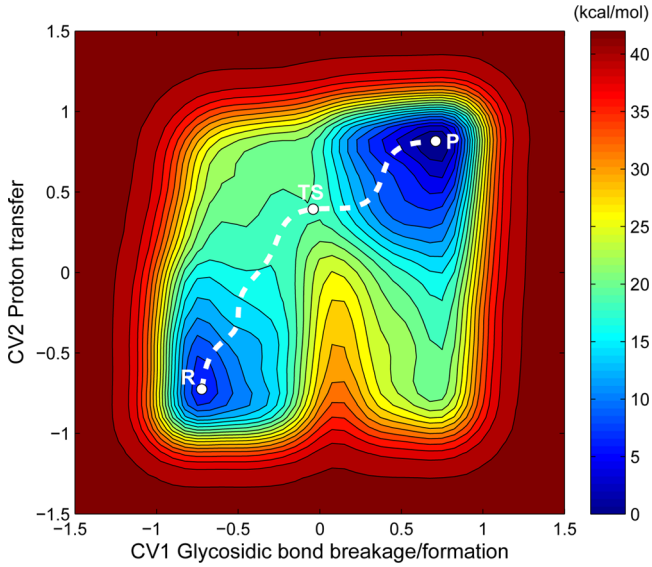

Figure 3. Free energy surface of melibiose hydrolysis by human α-galactosidase. The lowest free energy pathway is shown by a dashed line. Contours are separated by 2 kcal·mol^{-1}.

MFEP. The reaction had a free energy barrier of 13.4 kcal·mol^{-1}, and was exothermic by 6.3 kcal·mol^{-1}.

Snapshots of representative states along the reaction pathway are depicted in Figure 4. Table 2 shows the average distances and Mulliken charges of relevant atoms computed from all configurations falling into a small region around the stationary point of the FES (Figure 3) for structures that correspond to the reactant, TS, and product states. Complementing this information, Figure 5 shows the evolution of the main distances involving the anomeric carbon (C1′−O6, C1′−O_B, H_A−O6, H_A−O_A, and C1′−O5′), as well as atomic charges of C1′, O5′, and O6 along the reaction pathway. At the reactant state, the catalytic acid/base (Asp231) is in its protonated state, forming a weak hydrogen bond (2.43 Å) with the glycosidic oxygen atom (O6), and the nucleophile (Asp170) is in its charged state and is significantly separated (3.25 Å) from the C1′ atom (Table 2).

The reaction starts with the migration of the proton from Asp231 to the scissile glycosidic oxygen atom. When the proton transfers in the midway (CV1 = 0), the glycosidic bond elongates slightly from 1.45 to 1.68 Å. The system then reaches the TS when the scissile bond elongates to 2.12 Å and the distance between the nucleophile, Asp170, and the C1′ atom shortens from 3.25 Å in the reactant state to 2.35 Å in the TS. The Asp231 proton transfers further to within 1.13 Å of O6. When following the variation of distance along the MFEP (Figure 5), it suggests that the leaving group (the oxygen of the glycosidic linkage) dissociates more quickly than the nucleophile (Asp170) associates to form a bond. And considering the oxocarbenium ion like character of the TS (see below), the reaction appears to follow a D_N*A_N-like mechanism.

The reaction TS is characterized by a short intraring C1′−O5′ bond (it shrinks from 1.39 to 1.27 Å from R to TS), indicating the formation of a partial double bond, and an increased charge on the anomeric carbon (from 0.29 to 0.42 e). The in-plane configuration of the C2′, C1′, O5′, and C5′ atoms at the TS is consistent with sp2 hybridization of C1′ (see Figure 4). All of these changes reveal the presence of a species

dx.doi.org/10.1021/jp308747c | J. Phys. Chem. B XXXX, XXX, XXX−XXX

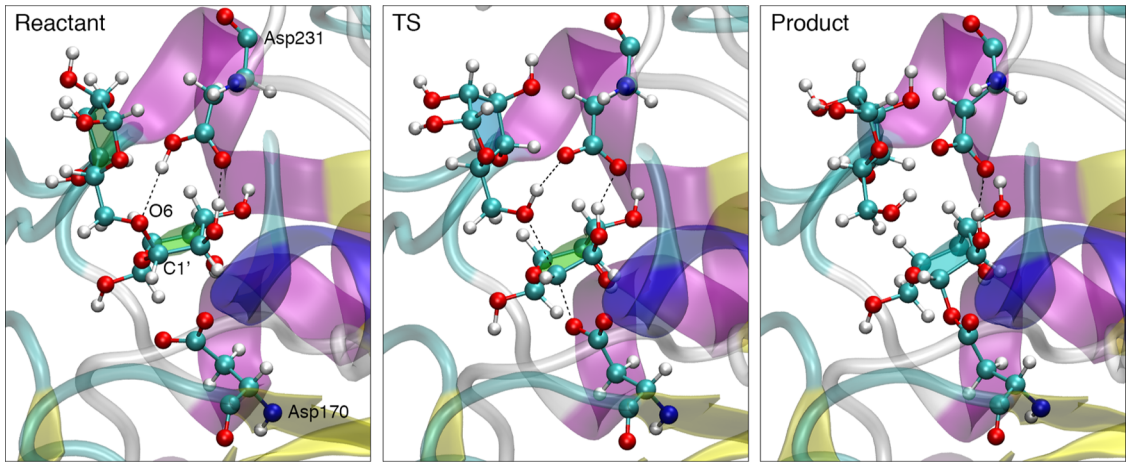

Figure 4. Representative snapshots along the reaction pathway, corresponding to the stationary points of the reaction free energy surface.

Table 2. Structural and Electronic Parameters at Different Stages of the Reaction Pathway

	reactant	TS	product
	Distance (Å)		
C1′−O6	1.45 ± 0.02	2.12 ± 0.32	3.22 ± 0.24
C1′−O_B	3.25 ± 0.16	2.35 ± 0.24	1.45 ± 0.01
H_A−O6	2.43 ± 0.41	1.13 ± 0.02	0.96 ± 0.01
H_A−O_A	1.01 ± 0.02	1.72 ± 0.22	3.00 ± 0.42
C1′−O5′	1.39 ± 0.02	1.27 ± 0.01	1.40 ± 0.01
	Charge (e)		
C1′	0.29 ± 0.01	0.42 ± 0.03	0.34 ± 0.00
O5′	−0.47 ± 0.02	−0.29 ± 0.02	−0.47 ± 0.00
O6	−0.58 ± 0.02	−0.67 ± 0.05	−0.67 ± 0.03

with oxocarbenium ion like character. Unlike GH16[24] and GH43,[29] the TS almost coincides with the point of maximal oxocarbenium ion like character (Figure 5).

The TS then collapses to the products, where the glycosidic oxygen atom (O6) is now 3.22 Å away from the C1′ atom, and the nucleophilic Asp170 forms a covalent bond of 1.45 Å with the anomeric carbon. The C1′ atom recovers sp3 hybridization with a C1′−O5′ distance of 1.40 Å.

Conformational Itinerary of Human α-Galactosidase. To analyze in detail the conformations of the galactoside unit of the substrate during the reaction, we extracted the puckering coordinates of all configurations along the predicted reaction pathway (Figure 6 and Table 3) and projected them over Stoddart's diagram. The puckering coordinates of the stationary points of the reaction FES (Table 3) well correspond to the itinerary predicted from the available Michaelis complex structures and glycosyl−enzyme intermediates of galactosidase ($^4C_1 \rightarrow [^4H_3]^{\ddagger} \rightarrow {}^1S_3$).[10] However, the detailed reaction itinerary is not a radial straight line on Stoddart's diagram but a warped one (Figure 6).[24] As the reaction proceeds, the galactoside first goes along the $^4C_1 \rightarrow E_3$ direction, and then moves toward $^4H_3$ before the TS state, and finally reaches the $^1S_3$ at the product state. Thus, the precise itinerary is $^4C_1 \rightarrow [E_3/^4H_3]^{\ddagger} \rightarrow {}^1S_3$.

CONCLUSION

In this study, we investigated the glycosylation step of human α-galactosidase by employing QM/MM metadynamics simulation. The results show that the glycosylation reaction follows

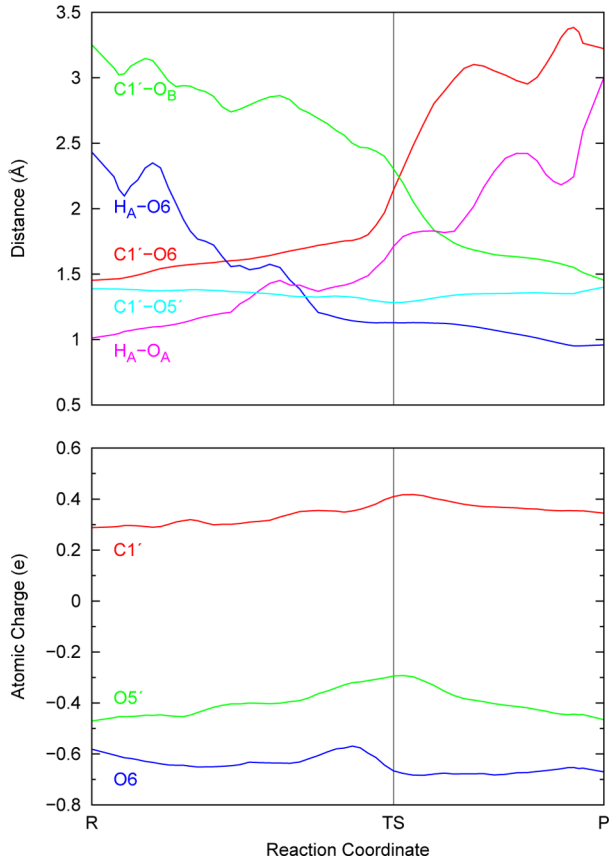

Figure 5. Variation of the relevant distances (C1′−O6, C1′−O_B, H_A−O6, H_A−O_A, and C1′−O5′) and atomic charges (C1′, O5′, and O6) along the reaction pathway. The plot is smoothed by a moving average over five data values.

a D_N*A_N-like mechanism, in which Asp231 acts as a proton donor and protonates the glycosidic oxygen while Asp170 plays the role of a nucleophile, attacking the anomeric center to form a glycosyl−enzyme intermediate, consistent with the previously proposed mechanism. It is shown that the TS has a substantial oxocarbenium ion character with an increased charge on the C1′ atom and a shorter C1′−O5′ bond. As the reaction proceeds, the galactoside ring of the substrate follows a conformational itinerary of $^4C_1 \rightarrow [E_3/^4H_3]^{\ddagger} \rightarrow {}^1S_3$, which is in

dx.doi.org/10.1021/jp308747c | J. Phys. Chem. B XXXX, XXX, XXX−XXX

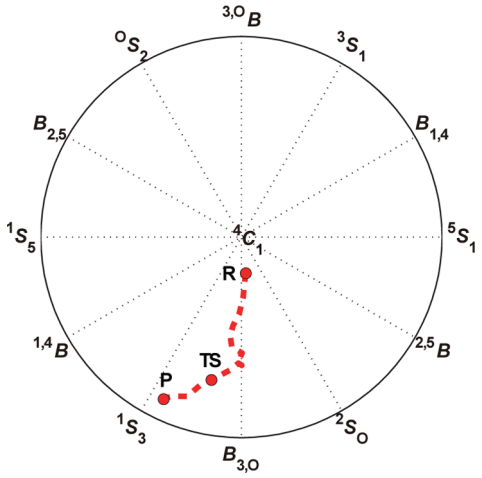

Figure 6. Reaction path of the glycosylation reaction projected onto Stoddart's diagram (i.e., conformational itinerary of the galactosyl ring), obtained from the puckering coordinates of all configurations along the predicted reaction pathway.

Table 3. Values of the Puckering Coordinates of the Substrate at Different Stages of the Reaction Pathway

	Q	θ	ϕ
R	0.58	10.5	173.3
TS	0.49	50.2	196.5
P	0.60	64.1	205.6

accordance with the available crystal structures of the reaction intermediates.

AUTHOR INFORMATION

Corresponding Author

*E-mail: ljy121@jlu.edu.cn.

Notes

The authors declare no competing financial interest.

ACKNOWLEDGMENTS

This work was supported by the National Natural Science Foundation of China (20973077), the Program for New Century Excellent Talents in University (NCET). The authors are grateful to the referees for their valuable comments on improving the manuscript.

REFERENCES

(1) Cantarel, B. L.; Coutinho, P. M.; Rancurel, C.; Bernard, T.; Lombard, V.; Henrissat, B. *Nucleic Acids Res.* **2009**, *37*, 233−238.
(2) Koshland, D. E. *Biol. Rev.* **1953**, *28*, 416−436.
(3) Sinnott, M. L. *Chem. Rev.* **1990**, *90*, 1171−1202.
(4) Garman, S. C.; Garboczi, D. N. *J. Mol. Biol.* **2004**, *337*, 319−335.
(5) Brady, R. O.; Gal, A. E.; Bradley, R. M.; Martensson, E.; Warshaw, A. L.; Laster, L. *N. Engl. J. Med.* **1967**, *276*, 1163−1167.
(6) Desnick, R. J.; Ioannou, Y. A.; Eng, C. M. In *The Metabolic and Molecular Bases of Inherited Disease*, 8th ed.; Scriver, C. R., Beaudet, A. L., Sly, W. S., Valle, D., Eds.; McGraw-Hill: New York, 2001; Vol. 3, pp 3733−3774.
(7) Frustaci, A.; Chimenti, C.; Ricci, R.; Natale, L.; Russo, M. A.; Pieroni, M.; Eng, C. M.; Desnick, R. J. *N. Engl. J. Med.* **2001**, *345*, 25−32.
(8) Asano, N.; Ishii, S.; Kizu, H.; Ikeda, K.; Yasuda, K.; Kato, A.; Martin, O. R.; Fan, J. Q. *Eur. J. Biochem.* **2000**, *267*, 4179−4186.
(9) Fan, J. Q.; Ishii, S.; Asano, N.; Suzuki, Y. *Nat. Med.* **1999**, *5*, 112−115.
(10) Guce, A. I.; Clark, N. E.; Salgado, E. N.; Ivanen, D. R.; Kulminskaya, A. A.; Brumer, H., III; Garman, S. C. *J. Biol. Chem.* **2010**, *285*, 3625−3632.
(11) Wang, J.; Hou, Q.; Sheng, X.; Gao, J.; Liu, Y.; Liu, C. *Int. J. Quantum Chem.* [Online early access]. DOI: 10.1002/qua.24131. Published Online: Apr 13, **2012**.
(12) Brás, N. F.; Moura-Tamames, S. A.; Fernandes, P. A.; Ramos, M. J. *J. Comput. Chem.* **2008**, *29*, 2565−2574.
(13) Brás, N. F.; Fernandes, P. A.; Ramos, M. J. *J. Chem. Theory Comput.* **2010**, *6*, 421−433.
(14) Brás, N. F.; Ramos, M. J.; Fernandes, P. A. *J. Mol. Struct.: THEOCHEM* **2010**, *946*, 125−133.
(15) Liu, J.; Wang, X.; Xu, D. *J. Phys. Chem. B* **2010**, *114*, 1462−1470.
(16) Saharay, M.; Guo, H.-B.; Smith, J. C.; Guo, H. QM/MM Analysis of Cellulase Active Sites and Actions of the Enzymes on Substrates. In *Computational Modeling in Lignocellulosic Biofuel Production*; Nimlos, M. R., Crowley, M. F., Eds.; ACS Symposium Series 1052; American Chemical Society: Washington, DC, 2011; pp 135−154.
(17) Li, J.; Du, L.; Wang, L. *J. Phys. Chem. B* **2010**, *114*, 15261−15268.
(18) Yan, S.; Li, T.; Yao, L. *J. Phys. Chem. B* **2011**, *115*, 4982−4989.
(19) Barnett, C. B.; Wilkinson, K. A.; Naidoo, K. J. *J. Am. Chem. Soc.* **2011**, *133*, 19474−19482.
(20) Soliman, M. E. S.; Ruggiero, G. D.; Pernía, J. J. R.; Greig, I. R.; Williams, I. H. *Org. Biomol. Chem.* **2009**, *7*, 460−468.
(21) Soliman, M. E. S.; Pernía, J. J. R.; Greig, I. R.; Williams, I. H. *Org. Biomol. Chem.* **2009**, *7*, 5236−5244.
(22) Li, J.; Wang, L. *Polym. Degrad. Stab.* **2011**, *96*, 1009−1014.
(23) Liu, J.; Zhang, C.; Xu, D. *J. Mol. Graphics Modell.* **2012**, *37*, 67−76.
(24) Biarnés, X.; Ardèvol, A.; Iglesias-Fernández, J.; Planas, A.; Rovira, C. *J. Am. Chem. Soc.* **2011**, *133*, 20301−20309.
(25) Jitonnom, J.; Lee, V. S.; Nimmanpipug, P.; Rowlands, H. A.; Mulholland, A. J. *Biochemistry* **2011**, *50*, 4697−4711.
(26) Passos, S.; Fernandes, P.; Ramos, M. *Theor. Chem. Acc.* **2011**, *129*, 119−129.
(27) Bottoni, A.; Miscione, G. P.; Vivo, M. D. *Proteins* **2005**, *59*, 118−130.
(28) Bowman, A. L.; Grant, I. M.; Mulholland, A. J. *Chem. Commun.* **2008**, 4425−4427.
(29) Petersen, L.; Ardèvol, A.; Rovira, C.; Reilly, P. J. *J. Am. Chem. Soc.* **2010**, *132*, 8291−8300.
(30) Greig, I. R.; Williams, I. H. *Chem. Commun.* **2007**, 3747−3749.
(31) Lameira, J.; Alves, C. N.; Tuñón, I.; Martí, S.; Moliner, V. *J. Phys. Chem. B* **2011**, *115*, 6764−6775.
(32) Petersen, L.; Ardèvol, A.; Rovira, C.; Reilly, P. J. *J. Phys. Chem. B* **2009**, *113*, 7331−7339.
(33) Barker, I. J.; Petersen, L.; Reilly, P. J. *J. Phys. Chem. B* **2010**, *114*, 15389−15393.
(34) Saharay, M.; Guo, H.; Smith, J. C. *PLoS One* **2010**, *5*, e12947.
(35) Wang, J.; Sheng, X.; Zhao, Y.; Liu, Y.; Liu, C. *Biochim. Biophys. Acta, Proteins Proteonomics* **2012**, *1824*, 750−758.
(36) Davies, G. J.; Planas, A.; Rovira, C. *Acc. Chem. Res.* **2011**, *45*, 308−316.
(37) *Maestro*, version 9.3; Schrödinger, LLC: New York, 2012.
(38) Li, H.; Robertson, A. D.; Jensen, J. H. *Proteins* **2005**, *61*, 704−721.
(39) Case, D. A.; Darden, T. A.; Cheatham, T. E., III; Simmerling, C. L.; Wang, J.; Duke, R. E.; Luo, R.; Walker, R. C.; Zhang, W.; Merz, K. M.; et al. *AMBER 12*; University of California: San Francisco, CA, 2012.
(40) Stewart, J. J. P. *J. Mol. Model.* **2007**, *13*, 1173−1213.
(41) Jurečka, P.; Černý, J.; Hobza, P.; Salahub, D. *J. Comput. Chem.* **2007**, *28*, 555−569.
(42) Cornell, W. D.; Cieplak, P.; Bayly, C. I.; Gould, I. R.; Merz, K. M.; Ferguson, D. M.; Spellmeyer, D. C.; Fox, T.; Caldwell, J. W.; Kollman, P. A. *J. Am. Chem. Soc.* **1995**, *117*, 5179−5197.

(43) Hornak, V.; Abel, R.; Okur, A.; Strockbine, B.; Roitberg, A.; Simmerling, C. *Proteins: Struct., Funct., Bioinf.* **2006**, *65*, 712−725.
(44) Kirschner, K. N.; Yongye, A. B.; Tschampel, S. M.; Gonzalez-Outeirino, J.; Daniels, C. R.; Foley, B. L.; Woods, R. J. *J. Comput. Chem.* **2008**, *29*, 622−655.
(45) Jorgensen, W.; Chandrasekhar, J.; Madura, J.; Impey, R.; Klein, M. *J. Chem. Phys.* **1983**, *79*, 926−935.
(46) Darden, T.; York, D.; Pedersen, L. *J. Chem. Phys.* **1993**, *98*, 10089−10092.
(47) Ryckaert, J.; Ciccotti, G.; Berendsen, H. J. C. *J. Comput. Phys.* **1977**, *23*, 327−341.
(48) Laio, A.; Parrinello, M. *Proc. Natl. Acad. Sci. U.S.A.* **2002**, *99*, 12562−12566.
(49) Ensing, B.; Laio, A.; Parrinello, M.; Klein, M. L. *J. Phys. Chem. B* **2005**, *109*, 6676−6687.
(50) Bonomi, M.; Branduardi, D.; Bussi, G.; Camilloni, C.; Provasi, D.; Raiteri, P.; Donadio, D.; Marinelli, F.; Pietrucci, F.; Broglia, R. A.; et al. *Comput. Phys. Commun.* **2009**, *180*, 1961−1972.
(51) Řezáč, J.; Fanfrlík, J.; Salahub, D.; Hobza, P. *J. Chem. Theory Comput.* **2009**, *5*, 1749−1760.
(52) Weigend, F.; Häser, M. *Theor. Chem. Acc.* **1997**, *97*, 331−340.
(53) *TURBOMOLE*, version 6.3; TURBOMOLE GmbH: Karlsruhe, Germany, 2011.